

**SMASIS2014-7669**

## **EFFECTS OF SENSOR GEOMETRY ON THE STRESS-AVERAGED OUTPUT OF PVDF SENSORS IN TIRES**

**Leon M. Headings**

**Jungkyu Park**

**Marcelo J. Dapino\***

The Ohio State University, Department of Mechanical and Aerospace Engineering,  
NSF I/UCRC on Smart Vehicle Concepts  
Columbus, Ohio, USA

### **ABSTRACT**

Polyvinylidene fluoride (PVDF) sensors are attractive for use in tires due to their high sensitivity, fast response time, low cost, and ability to operate without power supplies or signal amplification. Based on sensor design, placement, and signal processing techniques, they may be used to determine tire parameters such as tire revolutions, footprint size, and cornering and traction conditions. PVDF sensors generate a voltage output that is related to the average stress acting on the sensor. For non-uniform distributions of stress over the sensor area, there can be a significant difference between the stress at a point and the average sensor stress calculated from the measured voltage. Understanding the effects of sensor geometry on sensor output is important for designing sensors for specific applications, such as tires. This paper presents analytical and numerical models for PVDF voltage output that are developed from the linear piezoelectric constitutive equations, with the average sensor stress modeled using a convolution of the stress input and the PVDF electrode shape. Parametric studies on rectangular, stepped, and triangular sensor shapes show the effects of sensor geometry on voltage output for PVDF sensors under sinusoidal and tire stress inputs.

**Keywords:** tire sensors, PVDF, piezoelectric, sensor geometry, stress averaging

### **1. INTRODUCTION**

#### **1.1 Tire Sensors**

Most tire sensors have been motivated by safety through real time driver notification of tire condition and the use of tire-road information for improved vehicle electronic stability control (ESC). Tire pressure monitoring systems (TPMS) have been mandated in the U.S. on all light vehicles produced since

September 2007 to notify drivers of low inflation pressure. While TPMS is a very important first step, sensors for other tire conditions and tire-road interaction parameters are being developed to further improve safety. In addition to tire pressure, drivers may be notified of tire conditions such as damage and treadwear. Similarly, accurate estimations of tire-road conditions such as tire forces, slip angle, and current and maximum friction coefficient can be used to enhance the performance of active vehicle safety systems such as antilock braking systems (ABS) and ESC [1-4].

Most tire sensor development has focused on measuring tire pressure due to the large market created by the requirement for TPMS systems in light vehicles. Typically, these systems use battery-powered pressure sensors in combination with a wireless transmitter. Other tire sensors have been considered, including accelerometers with complex algorithms to determine tire dynamics and specific parameters of interest [2,5]. Surface acoustic wave (SAW) sensors, consisting of interdigitated electrodes on a piezoceramic substrate, have been proposed to monitor tire deformation [6]. In addition, wireless SAW sensors have been investigated that receive a wireless signal and use that energy to return a modified signal based on the sensor's condition, without additional power [7]. Ultrasonic sensors mounted on the inside of the wheel rim have been used to measure the actual tire rolling radius [8]. In addition to traditional polyimide film strain sensors, low stiffness strain sensors have been developed for compatibility with tire rubber [9]. Tire strain sensing has also been proposed using changes in the electrical properties of the tire itself, including impedance between the steel belts [10] and capacitance changes extracted using a wireless oscillator circuit [11].

Another approach to measure strain in the tire is to embed magnets in the tire tread and use Hall sensors or low power InAs/GaSb sensors to detect magnet position relative to a sensor mounted on the innerliner [12]. A key issue with many of these sensor concepts is that they require continuous power while smart materials such as PVDF and piezoceramics, which

\* Contact author: dapino.1@osu.edu

are considered here, generate electrical charge in response to stress in the sensor. Therefore, they do not require external power.

## 1.2 PVDF Sensors

Polyvinylidene fluoride (PVDF) is a piezoelectric polymer that can act as a sensor or actuator by generating electrical charge in response to an applied stress or vice versa. Due to their low cost, high sensitivity, nanosecond response times, and ability to operate without power supplies or signal amplification, they make excellent sensors for many applications. PVDF sensors are particularly attractive for use in tires, where they may be bonded to the innerliner to detect tire strain. Based on sensor design, placement, and signal processing techniques, the sensor output may be used to determine tire parameters such as tire revolutions, footprint size, and cornering and traction conditions.

The piezoelectric behavior of PVDF can be described by the strain-field formulation of the linearized coupled constitutive relations as follows:

$$S_p = s_{pq}^D T_q + g_{kp} D_k, \quad (1)$$

$$E_i = g_{iq} T_q + \beta_{ik}^T D_k. \quad (2)$$

The state variables are strain  $S_p$ , stress  $T_q$ , electric field  $E_i$ , and electric displacement  $D_k$ . The material properties are compliance at constant electric displacement  $s_{pq}^D$ , piezoelectric voltage constant  $g_{iq}$ , and impermeability measured at constant stress  $\beta_{ik}^T$ . The tensor indices  $i$  and  $k$  take values of 1 through 3 while the tensor indices  $p$  and  $q$  take the values 1 through 6, representing 11, 22, 33, 12, 23 or 32, 31 or 13, and 12 or 21, respectively. The 1, 2, and 3 values indicate directions corresponding to the sensor length, width, and thickness, respectively. They also correspond to the x, y, and z Cartesian axes as shown in Figure 1.

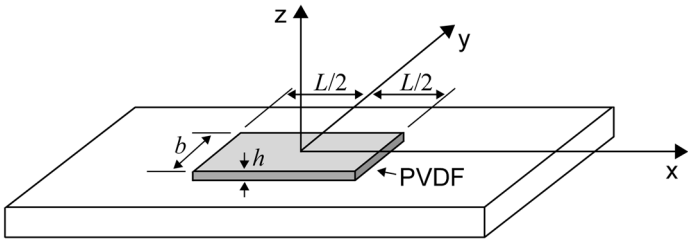


Figure 1. Diagram showing a PVDF sensor bonded to a fixed bar.

For the cases examined here, a PVDF sensor is considered with polarization along the 3-direction (thickness) and stress applied in the 1-direction (longitudinal). Stresses in the other directions are assumed to be negligible. If the input resistance of the measurement system is high enough for current flow across the electrodes to be negligible, then  $D \approx 0$  and equations (1) and (2) are decoupled. Since the electric field in the 3-

direction  $E_3$  can be expressed as the voltage  $V$  across the electrodes divided by the PVDF thickness  $h$ , the sensor output voltage can be written from (2) as

$$V(t) = g_{31} h T_{1,avg}(t). \quad (3)$$

The output voltage is proportional to the average stress acting on the sensor rather than the stress at a single point. Therefore, the stress calculated from the measured output voltage may be lower than the true maximum stress. It is necessary to understand the magnitude of this effect in order to select or design sensors that measure signals of interest with an acceptable deviation from the true maximum stresses present. While very small sensors could theoretically be used to minimize the effects of stress averaging, the low charge generated would significantly reduce the signal-to-noise ratio.

Kotian et al. [13] modeled the stress-averaged sensor output voltage for a rectangular sensor with both sinusoidal and impact forces acting on the end of a bar. The resulting stress waves traveled at the speed of sound for the bar material, so the wavelengths were much larger than typical sensor lengths for the range of frequencies used in structural sensing applications. The stress averaging effects were therefore fairly small for many common applications. In this paper, we examine stress inputs for a sensor bonded to the innerliner of a vehicle tire. In this case, as the tire rotates through a footprint, there are sharp fluctuations in stress, with the length of the fluctuations dictated by the tire size and deflection (load and inflation) rather than the speed of sound. This results in stress inputs with wavelengths similar to common sensor lengths, causing an attenuation of the output voltage due to stress averaging effects.

In order to examine the effects of sensor size and geometry for tire innerliner strain profiles, a general convolution model is developed and examined both analytically and numerically for the case of a sinusoidal stress input. The numerical model is then used to conduct a parametric study on the effects of sensor size and geometry on the output of a PVDF sensor bonded to the innerliner of a tire.

## 2. NOMENCLATURE

Symbol	Description	SI Unit
$A$	surface area (PVDF)	$m^2$
$D$	electric displacement	$C/m^2$
$E$	electric field	$V/m$
$L$	length (PVDF)	$m$
$S$	strain	-
$T$	stress	$Pa$
$V$	voltage	$V$
$Y$	elastic modulus	$Pa$
$g_{31}$	piezoelectric stress constant	$Vm/N$
$b$	width (PVDF)	$m$
$f$	frequency	$Hz$
$h$	thickness (PVDF)	$m$

$k$	wave number	rad/m
$p$	sensor shape function	m
$s^D$	compliance, measured at $D=0$ (PVDF)	1/Pa
$\beta^T$	impermissivity measured at $T=0$ (PVDF)	m/F
$\lambda$	wavelength	m
$t$	time	s
$\tau$	amplitude of sinusoidal stress input	Pa
$\omega$	angular frequency	rad/s

### 3. MODELING OF PVDF OUTPUT VOLTAGE FOR A SINUSOIDAL INPUT STRESS

The output voltage of a PVDF sensor is proportional to the average stress acting on the sensor. A variety of approaches may be used to determine the average stress acting on a sensor for different stress inputs and sensor geometries. Here, we present a convolution integral approach that can be readily applied to any type of input and sensor shape. This method is developed analytically for the case of a rectangular sensor and sinusoidal input stress in order to provide insight into the parameters that affect the sensor output and to validate the numerical model. Then, the numerical model is used to conduct parametric studies on different sensor geometries for the cases of sinusoidal stress inputs and typical tire innerliner stress profiles.

#### 3.1 Analytical Convolution Model of Output Voltage

A convolution integral represents the amount of overlap between one function and a second function that is shifted over it. Therefore, it can be used to determine the average stress on a sensor geometry based on the stress input and a sensor shape function. The convolution of a sensor stress input  $T(x,t)$  and sensor shape  $p(x)$  is mathematically defined as:

$$T(x,t) * p(x) = \int_{-\infty}^{\infty} T(\delta,t)p(x-\delta)d\delta. \quad (4)$$

This convolution can be interpreted as an integration of the stress input over the area of the sensor. To determine the average stress in the sensor, the convolution must be divided by the sensor area  $A$ .

If it is assumed that stresses in the 2 and 3 directions are negligible and that the measurement system's input resistance is high enough to consider the PVDF as an open circuit, then the constitutive relations are decoupled and the voltage output  $V(t)$  is represented by (3). While the convolution occurs over the spatial variable  $x$ , the voltage output corresponds to a fixed sensor location centered at  $x=0$ . The voltage output can therefore be written in terms of the convolution integral as

$$V(t) = \frac{g_{31}h}{A} \left[ \int_{-\infty}^{\infty} T_1(\delta,t)p(x-\delta)d\delta \right]_{x=0}. \quad (5)$$

#### 3.2 Analytical Model of Output Voltage for a Sinusoidal Longitudinal Stress Input and Rectangular Sensor

In general, a traveling sinusoidal stress wave can be expressed as

$$T_1(x,t) = \tau \sin(kx - \omega t), \quad (6)$$

with an amplitude  $\tau$ , wave number  $k$ , and angular frequency  $\omega$ .

For a rectangular sensor centered at  $x=0$  and having a width of  $b$  and length of  $L$ , the shape function  $p(x)$  can be written as a sum of two step functions to give a width of  $b$  at  $x > -L/2$  and return to a width of 0 at  $x > L/2$ ,

$$p(x) = bu \left( x + \frac{L}{2} \right) - bu \left( x - \frac{L}{2} \right). \quad (7)$$

Inserting (6) and (7) into (5), the voltage can be written

$$V(t) = \left\{ \int_{-\infty}^{\infty} \frac{g_{31}hb\tau}{A} \sin(k\delta - \omega t) \left[ u \left( x + \frac{L}{2} - \delta \right) - u \left( x - \frac{L}{2} - \delta \right) \right] d\delta \right\}_{x=0}. \quad (8)$$

Because of the step functions,

$$\begin{aligned} V(t) &= 0 \quad \text{for } x + \frac{L}{2} < \delta, \\ V(t) &= 0 \quad \text{for } \delta < x - \frac{L}{2}. \end{aligned} \quad (9)$$

For  $x - L/2 < \delta < x + L/2$ ,

$$\begin{aligned} V(t) &= \left[ \frac{g_{31}hb\tau}{A} \int_{x-L/2}^{x+L/2} \sin(k\delta - \omega t) d\delta \right]_{x=0} \\ &= \left\{ \frac{g_{31}hb\tau}{Ak} \cos \left[ k \left( x - \frac{L}{2} \right) - \omega t \right] - \frac{g_{31}hb\tau}{Ak} \cos \left[ k \left( x + \frac{L}{2} \right) - \omega t \right] \right\}_{x=0}. \end{aligned} \quad (10)$$

The area of the rectangular sensor is  $A=bL$ , so the width cancels out and does not affect the output voltage. Since  $\cos(\alpha \pm \beta) = \cos(\alpha)\cos(\beta) \mp \sin(\alpha)\sin(\beta)$ , we can let  $\alpha = kx - \omega t$  and  $\beta = kL/2$  to rewrite the voltage as

$$V(t) = \left[ \frac{2g_{31}h\tau}{Lk} \sin\left(\frac{kL}{2}\right) \sin(kx - \omega t) \right]_{x=0} \quad (11)$$

$$= \frac{2g_{31}h\tau}{Lk} \sin\left(\frac{kL}{2}\right) \sin(-\omega t).$$

Written in terms of wavelength and frequency, the voltage has the form

$$V(t) = \frac{g_{31}h\tau\lambda}{\pi L} \sin\left(\frac{\pi L}{\lambda}\right) \sin(-2\pi ft). \quad (12)$$

From (12) it can be seen that the rectangular sensor's output voltage is sinusoidal with the same frequency as the input stress. The amplitude is proportional to the sensor's piezoelectric constant, thickness, and stress amplitude. The amplitude also depends on the sensor length and wavelength of the stress input, as described in more detail in the next section.

Since the stress is assumed to be constant across the sensor width, changing the width of the sensor does not change the average stress on the sensor or the voltage output. However, for the same average stress, a larger sensor area will produce a higher charge output. It was previously noted that very short sensors would minimize the sensor averaging effect while greatly reducing the signal-to-noise ratio. Although the width does not affect the sensor-averaged voltage output, increasing the sensor width can help to improve the signal-to-noise ratio and offset reductions due to decreased sensor lengths.

### 3.3 Numerical Convolution Model of Output Voltage

Although the general analytical convolution model (5) can be solved analytically for simple sensor shapes and stress inputs, such as the rectangular sensor and sinusoidal input in section 3.2, the greatest benefit of the convolution approach is the ease of numerically modeling any arbitrary discretely-defined stress input and sensor shape.

The discrete convolution is defined as

$$T[n] * p[n] = \sum_{m=-\infty}^{\infty} T[m]p[n-m]. \quad (13)$$

Alternatively, pre-defined functions such as *conv* in Matlab may be used to compute the discrete convolution of two vectors. Just as the convolution integral was divided by the sensor area to give the average stress (5), the discrete Matlab convolution function must be divided by the average width of the sensor  $b_{avg}$  and the number of data points used to define the sensor shape ( $n_{pts}=L/\Delta x+1$ , where  $\Delta x$  is the spacing between data points),

$$V = \frac{g_{31}h}{b_{avg}\left(\frac{L}{\Delta x} + 1\right)} \text{conv}(T[n], p[n]). \quad (14)$$

## 4. PARAMETRIC STUDY ON SENSOR GEOMETRY FOR A SINUSOIDAL LONGITUDINAL STRESS INPUT

In order to examine the effects of sensor geometry on PVDF sensor output voltage, parametric studies are conducted using typical properties based on commercial PVDF film sensors produced by Measurement Specialties, Inc., as summarized in Table 1. For modeling purposes, an input stress amplitude of 1 MPa is used. Although this stress corresponds to a strain amplitude of only  $\tau/E_s=3.33\text{e-}4$ , from (3), it would produce an output voltage amplitude of 6.048 V for an infinitesimally small point sensor without any sensor averaging effects.

**Table 1. Properties of PVDF sensor and stress input.**

Symbol	Parameter	Value
$h$	PVDF film thickness	28 $\mu\text{m}$
$g_{31}$	Piezoelectric stress constant	0.216 $\frac{\text{V/m}}{\text{N/m}^2}$
$E_s$	Elastic modulus of the sensor	3 GPa
$\tau$	Amplitude of sinusoidal stress input	1 MPa

Using the numerical convolution model, the magnitude of the output voltage is calculated for the three sensor shapes described in Figure 2. While maintaining equal maximum lengths and widths among the shapes results in different average widths and total areas, which affect the output of a typical convolution integral, the formulation for voltage (14) is based on the average stress by dividing by average width and number of data points. Hence, changing the reference width  $b$  does not affect the voltage output. However, the variation in width presented by non-rectangular shapes acts to affect the weighting of different parts of the input stress signal.

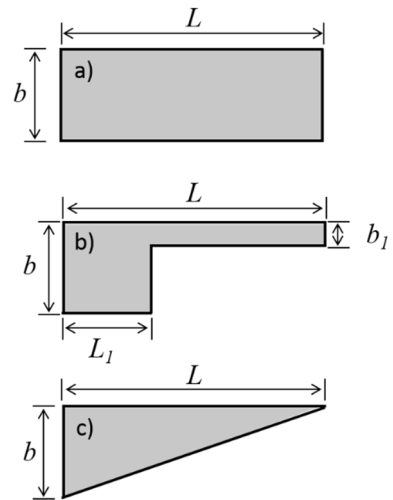


**Figure 2. Sensor shapes examined: a) rectangular, b) stepped, and c) triangular.**

#### 4.1 Rectangular Sensor Shape

The numerically-calculated magnitude of the output voltage for the rectangular sensor (Figure 2) is plotted in Figure 3 and confirmed to match the magnitude calculated from (12). When the rectangular sensor length is equal to a multiple of the wavelength of the sinusoidal stress input, the average stress is zero.

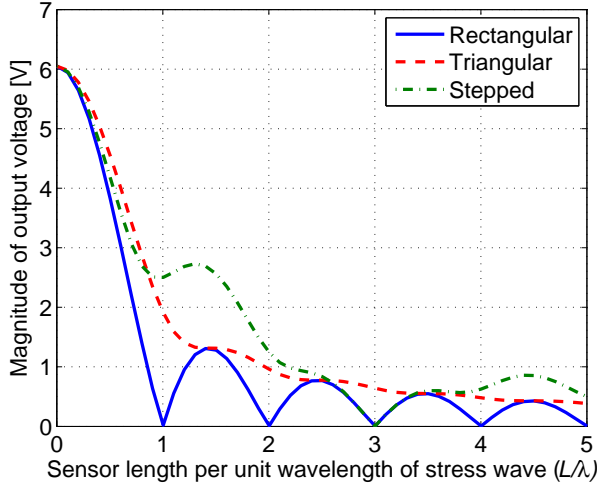


Figure 3. Magnitude of the sensor-averaged voltage due to a sinusoidal stress input for three sensor shapes.

#### 4.2 Stepped Sensor Shape

A stepped sensor shape as shown in Figure 2b is considered with  $L_I=L/3$  and  $b_I=b/4$ . The magnitude of the stepped sensor's voltage in Figure 3 decreases to zero when the length equals a multiple of three times the wavelength. This is expected since the stepped sensor acts as two rectangular sensors with lengths of  $L/3$  and  $2L/3$ . The stepped sensor shape with these dimensions provides a much lower stress-averaged voltage reduction than the other shapes up to  $L/\lambda=2$ . Therefore, we examine the effects of the step size  $b_I$  and location  $L_I$ , represented as fractions of  $b$  and  $L$ .

Figure 4-Figure 7 show the voltage outputs for step widths of  $b_I=0.1b$ ,  $0.3b$ ,  $0.5b$ , and  $0.7b$ , respectively. Comparing these plots, it is observed that as the width of the narrower step section increases and approaches  $b_I=b$ , the voltage approaches the response of a rectangular sensor.

Therefore, Figure 4 with a step width of  $b_I=0.1b$ , shows the greatest variation in response. While the rectangular sensor exhibits zero voltage at  $L/\lambda=1$ , a step location of  $L_I=0.1L$  maintains nearly 30% of the maximum output voltage at  $L/\lambda=5$ . As the step location decreases from  $L_I=0.9L$  to  $L_I=0.1L$ , the  $L/\lambda$  ratio at which the voltage approaches zero becomes larger, although the voltage reduction becomes less smooth. Compared with the response of a rectangular sensor, the step width and location of  $b_I=0.1b$  and  $L_I=0.5L$  offers a relatively smooth voltage reduction, approaching zero volts at  $L/\lambda=2$  and

maintaining around 50% of the maximum output voltage at  $L/\lambda=1$ .

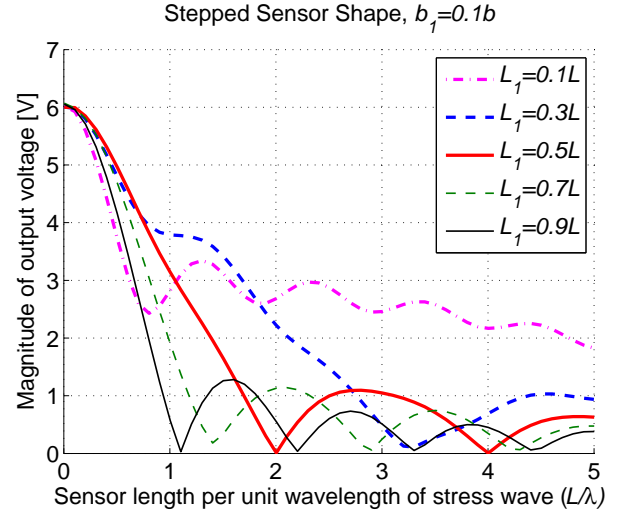


Figure 4. Magnitude of the sensor-averaged voltage due to a sinusoidal stress input for five step lengths with  $b_I=0.1b$ .

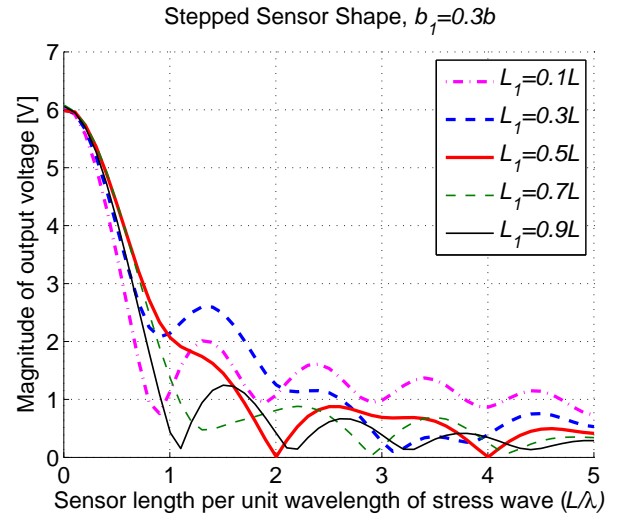


Figure 5. Magnitude of the sensor-averaged voltage due to a sinusoidal stress input for five step lengths with  $b_I=0.3b$ .

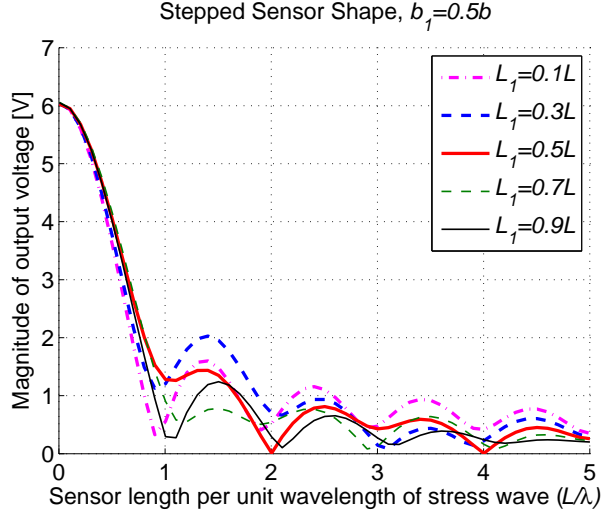


Figure 6. Magnitude of the sensor-averaged voltage due to a sinusoidal stress input for five step lengths with  $b_I=0.5b$ .

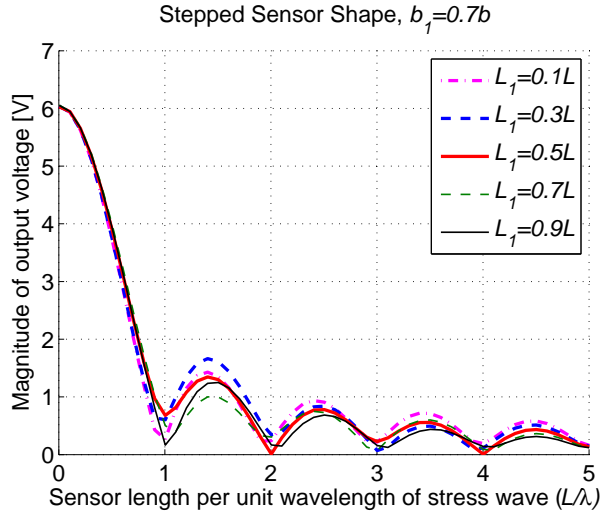


Figure 7. Magnitude of the sensor-averaged voltage due to a sinusoidal stress input for five step widths with  $b_I=0.7b$ .

Since different rectangular sensors have different response characteristics, one can consider two rectangles with equally weighted contributions to the overall output. Figure 8 shows the voltage response as the step width is varied for each step location to maintain equal areas between the two rectangles. It is observed that this has the effect of maintaining a similar response profile to a singular rectangular sensor (the case of  $b_I=1b$  in the plot), with the different dimensions affecting the overall slope of the voltage reduction. Of the cases shown, the geometry with  $L_I=0.1L$  and  $b_I=0.11b$  shows the least voltage reduction, maintaining about 30% of the maximum voltage at  $L/\lambda=5$ .

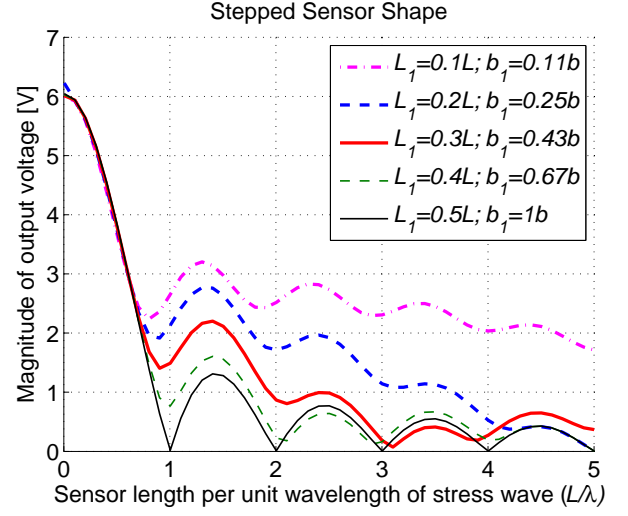


Figure 8. Magnitude of the sensor-averaged voltage due to a sinusoidal stress input for five step widths with  $b_I$  adjusted such that the two rectangles with length  $L_I$  and  $1-L_I$  have the same area. Note that  $L_I=0.5L$ ,  $b_I=1b$  is a rectangular (non-stepped) shape.

### 4.3 Triangular Sensor Shape

A triangular sensor as shown in Figure 2c produces the voltage amplitude shown in Figure 3. For purely sinusoidal input stresses, the triangular sensor has the advantage of providing a smoother reduction in sensor-averaged voltage. It reduces from the maximum of around 6 V to 0.4 V at  $L/\lambda=5$ .

### 4.4 Discussion of Results

For sinusoidal input stresses, the best geometry depends on the design requirements of a specific application. In particular, the choice would depend on sensor length and width limitations, signal-to-noise requirements, and stress wavelengths of interest. The triangular sensor does not have  $L/\lambda$  values that produce zero output voltage; therefore, it is better than a rectangular sensor with respect to sensor-averaged voltage reductions. However, the width would need to be doubled in order to maintain a comparable signal-to-noise ratio.

If there is a limit on the wavelengths of interest for a given sensor length, then a stepped sensor may be designed to minimize the sensor-averaged voltage reduction up to the targeted  $L/\lambda$  ratio. While the plots above only illustrate a range of responses, the smaller step width of  $0.1L$  provides less attenuation of the output voltage due to stress averaging.

## 5. PARAMETRIC STUDY ON SENSOR GEOMETRY FOR A TIRE STRESS INPUT

In order to examine the effects of sensor geometry on output voltage for a tire stress input, it is assumed that the PVDF sensor is bonded to the innerliner of a tire at the center

of the tread area. A circumferential strain profile (Figure 9) is generated by a finite element model of a tire. The circumference is considered to be 3 m, which is representative of a typical truck-bus tire. The wavelength  $\lambda$  of the tire input equals the tire circumference. While the PVDF sensor's stiffness may not be negligible compared to the stiffness of the innerliner, for the purposes of this analysis it is assumed that the free strain at the innerliner surface equals the strain of the PVDF sensor. A reduction in strain due to the stiffness of the sensor would reduce the scale of the voltage output, but would not change the effects of sensor geometry. The stress input to the sensor is calculated as this periodic strain profile, divided by the elastic modulus specified in Table 1. The numerical convolution model is used to examine the stress-averaged output voltage for the tire-induced sensor stress input and the three sensor shapes shown in Figure 2.

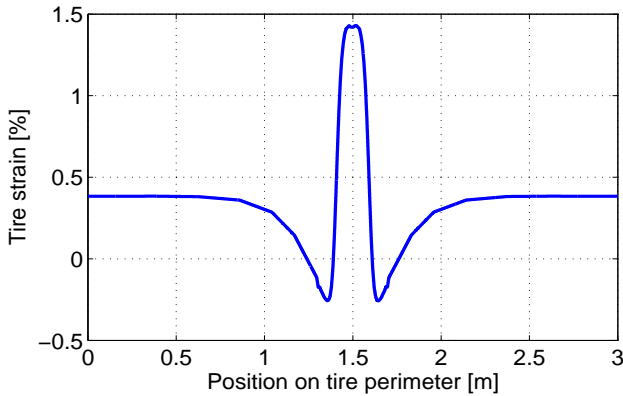


Figure 9. Strain on the innerliner surface of a tire at the center of the tread area.

## 5.1 Rectangular Sensor Shape

The magnitude of the voltage output by a rectangular sensor is plotted in Figure 10. Since  $\lambda$  represents the tire circumference,  $2\lambda$  represents a sensor on the innerliner that wraps around the tire circumference twice. Since the stress profile is not symmetric about the x-axis, there are no  $L/\lambda$  values where the magnitude of the output goes to zero. However, when the sensor length equals a multiple of the wavelength (tire circumference), the voltage output remains constant at 63 V, which is approximately 25% of the maximum voltage of 259 V for a point sensor with no stress averaging. The maximum strain of 1.43% is multiplied by the elastic modulus of the sensor  $E_s$  to find the maximum stress of 42.9 MPa. Using this stress in (3) gives the calculated maximum voltage of 259 V, which agrees with the maximum from the numerical convolution model results plotted in Figure 10.

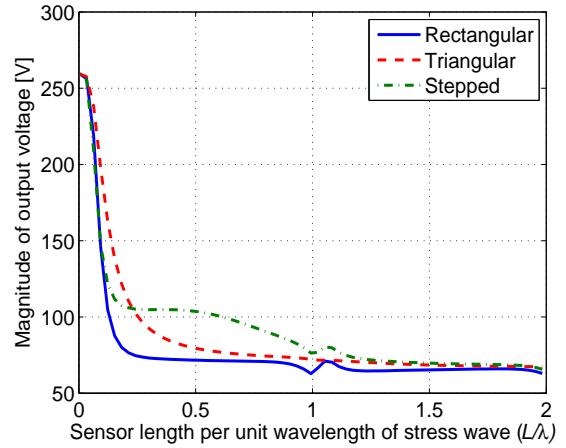


Figure 10. Magnitude of the sensor-averaged voltage due to a tire-induced stress input for three sensor shapes.

For the sinusoidal stress input case, the convolved average stress was simply a sinusoid with a reduced amplitude. For the non-sinusoidal tire-induced stress case, the shape of the convolved average stress changes as the length of the rectangular sensor is increased. Figure 11 shows how the shape changes with sensor length. The stress becomes constant when  $L/\lambda=1$  ( $L=3$  m). Therefore, while neglecting the effects of sensor averaging for a sinusoidal input may lead to an underestimation of the true stress amplitude, neglecting the effects of sensor averaging for a non-sinusoidal input such as a tire stress profile also leads to a distorted measurement of the stress profile. This is particularly important for applications such as tire measurements, where the objective is not just to identify the maximum stress, but to examine the characteristics of the signal to determine information such as footprint size, cornering and traction conditions, impact events, and irregular wear.

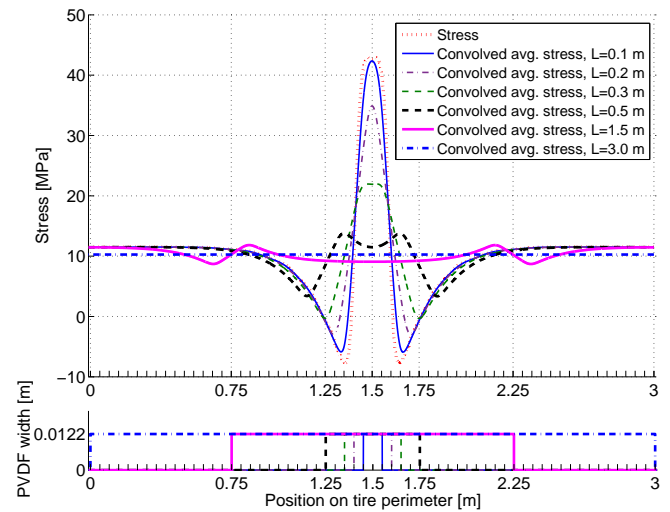


Figure 11. Sensor stress and convolved stress profiles for six rectangular sensor lengths with  $\lambda=3$  m. The lower plot shows the rectangular PVDF shapes that were convolved with the sensor stress.



## 5.2 Stepped Sensor Shape

As with the sinusoidal input case, a stepped sensor shape (Figure 2b) is considered with  $L_I=L/3$  and  $b_I=b/4$  for the tire stress input. The magnitude of the stepped sensor's voltage in Figure 10 is larger than the output of the rectangular and triangular sensors from  $0.23 < L/\lambda < 1$ . However, as discussed in the previous subsection, the shape of the output profile is also important for identifying certain tire conditions.

As with the sinusoidal input, the greatest effect on the sensor averaged voltage occurs with larger width differences, such as  $b_I=0.1b$ , and step locations such as  $L_I=0.1L$ . This is illustrated by Figure 12 and Figure 13.

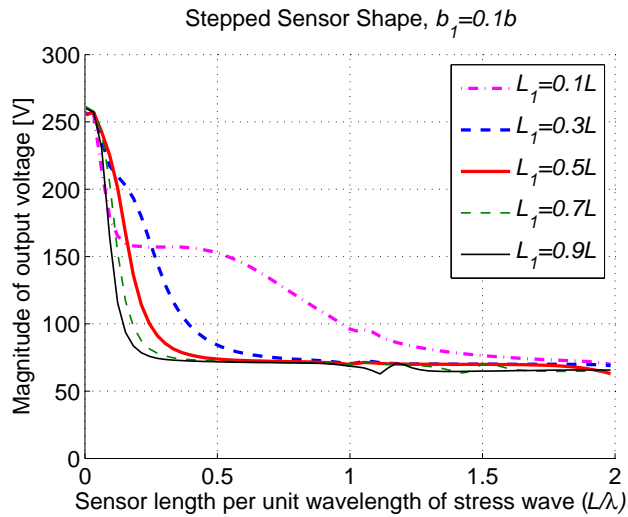


Figure 12. Magnitude of the sensor-averaged voltage due to a tire-induced stress input for five step widths with  $b_I=0.1b$ .

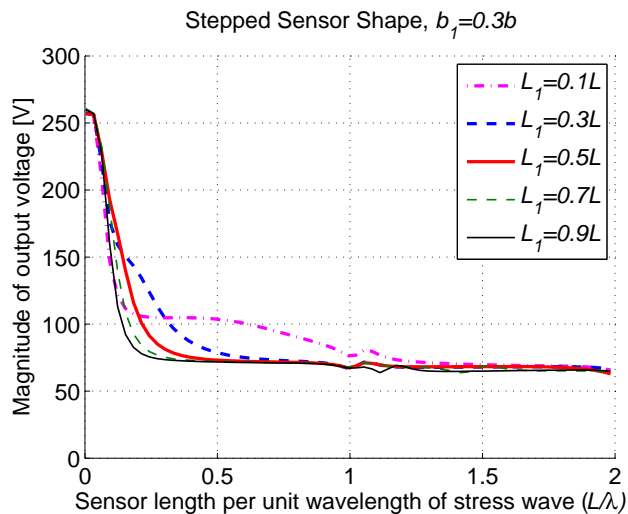


Figure 13. Magnitude of the sensor-averaged voltage due to a tire-induced stress input for five step widths with  $b_I=0.3b$ .

Figure 14 shows the convolved average stress for a stepped sensor with  $b_I=0.1b$ ,  $L_I=0.1L$ , and varying sensor lengths. Unlike the convolution with the rectangular sensor, the stepped shape gives an asymmetric convolution output. The desirability of this depends on what tire characteristics are being identified. For example, the asymmetry with  $L=0.5$  m is distinctive enough to determine the direction of tire rotation. While the convolved stress for a rectangular sensor with the same length is symmetric, it exhibits a greater reduction in sensor averaged magnitude.

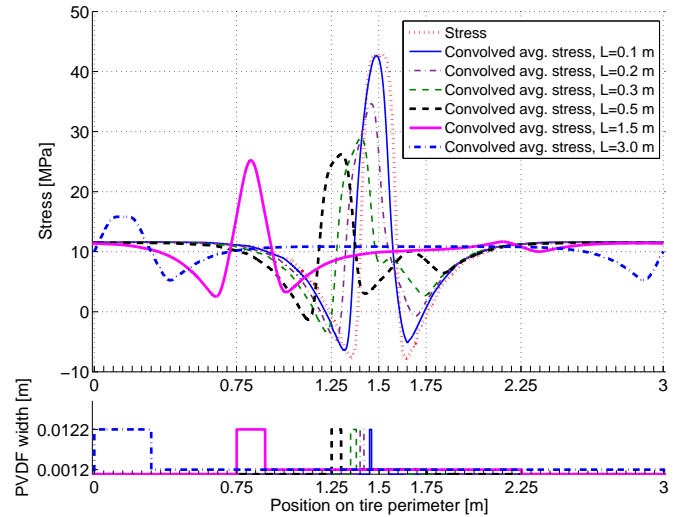
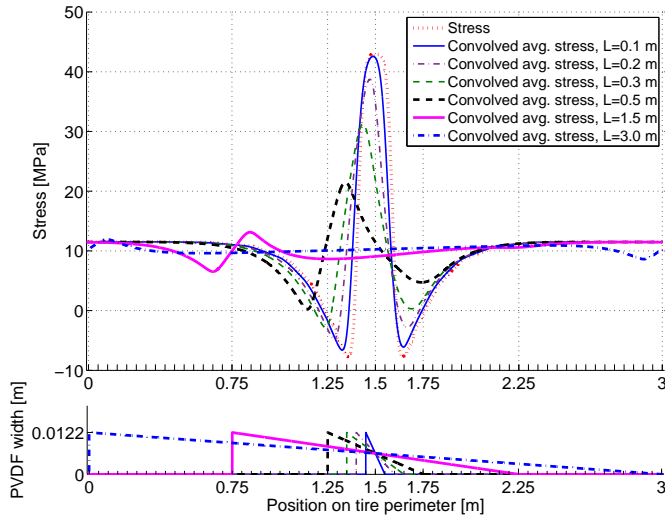


Figure 14. Sensor stress and convolved stress profiles for six stepped sensor lengths with  $\lambda=3$  m. The lower plot shows the stepped PVDF shapes that were convolved with the sensor stress. While length was varied,  $b_I=0.1b$  and  $L_I=0.1L$  for each.

## 5.3 Triangular Sensor Shape

A triangular sensor (Figure 2c) is examined for the case of the tire-induced stress input. The magnitude of the output voltage is shown in Figure 10. As with the sinusoidal input stresses, the triangular sensor has the advantage of providing a smoother reduction in sensor-averaged voltage than a rectangular or stepped sensor. Although the triangular sensor produces a greater output voltage than a rectangular sensor for all sensor lengths, a stepped sensor can be designed to produce a greater output voltage at longer sensor lengths ( $L/\lambda > 0.23$  for the dimensions shown). As with the asymmetric stepped sensor, the triangular sensor's convolved stress output is asymmetric (Figure 15). Although the magnitude is higher for the stepped sensor at longer sensor lengths such as  $L=1.5$  m, the triangular sensor provides a more consistent asymmetric response profile and smoother magnitude reduction, which would simplify the development of algorithms to identify characteristics such as the direction of tire rotation.





**Figure 15. Sensor stress and convolved stress profiles for six triangular sensor lengths with  $\lambda=3$  m. The lower plot shows the triangular PVDF shapes that were convolved with the sensor stress.**

## 5.4 Discussion of Results

For tire-induced stress inputs, the best sensor geometry depends on the design requirements of a specific application as well as the characteristics of interest, such as footprint size, cornering and traction conditions, impact events, and irregular wear. Although a sinusoidal stress input results in a sinusoidal convolved average stress for any rectangular sensor, the length of the rectangular sensor can affect the shape of the convolved average stress for non-sinusoidal stress inputs such as those found in tires.

For tire rotation inputs, a rectangular sensor does not produce a voltage of zero for any sensor length. However, the sensor output approaches a constant voltage when the sensor length equals a multiple of the wavelength (tire circumference), which is not useful for identifying tire characteristics. The rectangular sensor produces a symmetric voltage output profile, but exhibits a larger sensor averaged voltage reduction than stepped or triangular sensors. Although a stepped sensor can be designed to generate an output with lower voltage reduction than a triangular sensor, the triangular sensor provides a more consistent asymmetric response profile for different sensor lengths. This makes the triangular sensor better for identifying characteristics such as the direction of tire rotation.

## 6. CONCLUSIONS

Polyvinylidene fluoride (PVDF) sensors are attractive for use in tires due to their high sensitivity, fast response time, low cost, and ability to operate without power supplies or signal amplification. Based on sensor design, placement, and signal processing techniques, they may be used to determine tire

parameters such as tire revolutions, footprint size, and cornering and traction conditions.

Because PVDF sensors generate a voltage output that is related to the average stress acting on the sensor, non-uniform distributions of stress over the sensor area can lead to significant differences between the stress at a point and the average sensor stress calculated from the measured voltage. In order to analyze the effects of sensor stress averaging, analytical and numerical models were presented to calculate the output voltage using the linear piezoelectric equations and a convolution of the stress input and PVDF sensor shape.

The numerical convolution model can be readily used to evaluate the sensor averaging effects for any arbitrary stress input and sensor geometry. Parametric studies were conducted on rectangular, stepped, and triangular sensor shapes to examine their effects on sinusoidal and tire-induced stress inputs. Although the sensor geometry only affects the magnitude of the stress averaged voltage for sinusoidal stress inputs, it also affects the response profile for non-sinusoidal inputs such as the sensor stress resulting from the innerliner strain profile around the circumference of a tire.

The choice of sensor geometry and size depend on sensor length and width limitations, signal-to-noise requirements, stress wavelengths of interest, and the signal characteristics being identified. For example, of the geometries considered here, rectangular sensors provide the stress averaged output that best represents the profile of the actual stress while stepped sensors can be designed to provide the largest voltage magnitudes over a wide range of sensor lengths. The smooth asymmetry of triangular sensors would be the best choice for identifying the direction of tire rotation. Smaller sensors are better for identifying the maximum stresses present, but require a trade-off with respect to the signal-to-noise ratio. Larger sensors are better for identifying characteristics such as the direction of tire rotation where sensor averaging is needed in order to achieve an asymmetric voltage output from a symmetric input stress profile.

## ACKNOWLEDGMENTS

The authors would like to acknowledge the financial support by the member organizations of the Smart Vehicle Concepts Center ([www.SmartVehicleCenter.org](http://www.SmartVehicleCenter.org)), a National Science Foundation Industry/University Cooperative Research Center. Financial and technical support was received from Bridgestone Americas Tire Operations.

## REFERENCES

- [1] Arat, M. A., Singh, K., and Taheri, S., 2013, "Optimal Tire Force Allocation by Means of Smart Tire Technology," *SAE Int. J. of Passenger Cars – Mechanical Systems*, 6(1), pp. 163–176.

- [2] Ergen, S. C., Sangiovanni-Vincentelli, A., Sun, X., Tebano, R., Alalusi, S., Audisio, G., and Sabatini, M., 2009, "The Tire as an Intelligent Sensor," *IEEE Trans. on Computer-Aided Design of Integrated Circuits and Systems*, 28(7), pp. 941–955.
- [3] Uchanski, M., Hedrick, K., and Müller, S., 2003, "Estimation of the Maximum Tire-Road Friction Coefficient," *J. of Dynamic Systems, Measurement, and Control*, 125(4), pp. 607–617.
- [4] Apollo Final Report, 2005, "Intelligent Tyre for Accident-Free Traffic", IST-2001-34372, The Apollo Consortium.
- [5] Savaresi, S. M., Tanelli, M., Langthaler, P., and del Re, L., 2008, "New Regressors for the Direct Identification of Tire Deformation in Road Vehicles Via "In-Tire" Accelerometers," *IEEE Trans. on Control Systems Technology*, 16(4), pp. 769–780.
- [6] Pohl, A., Steindl, R., and Reindl, L., 1999, "The 'Intelligent Tire' Utilizing Passive SAW Sensors Measurement of Tire Friction," *IEEE Trans. on Instrumentation and Measurement*, 48(6), pp. 1041–1046.
- [7] Stelzer, A., Schimetta, G., Reindl, L., Springer, A., and Weigel, R., 2001, "Wireless SAW-Sensors for Surface and Subsurface Sensing Applications," *Proc. of SPIE's 46th Annual Meeting, Int. Conf. on Subsurface Sensing Technologies and Applications III*, 4491, pp. 358-366.
- [8] Magori, V., Magori, V. R., and Seitz, N., 1998, "On-line Determination of Tyre Deformation, a Novel Sensor Principle," *Proc. of IEEE Ultrasonics Symposium*, 1, pp. 485-488.
- [9] Matsuzaki, R., Keating, T., Todoroki, A., and Hiraoka, N., 2008, "Rubber-Based Strain Sensor Fabricated Using Photolithography for Intelligent Tires," *Sensors and Actuators A: Physical*, 148(1), pp. 1–9.
- [10] Sergio, M., Manaresi, N., Tartagni, M., Canegallo, R., and Guerrieri, R., 2006, "On a Road Tire Deformation Measurement System Using a Capacitive-Resistive Sensor," *Smart Mater. Struct.*, 15(6), pp. 1700-1706.
- [11] Matsuzaki, R., and Todoroki, A., 2005, "Passive Wireless Strain Monitoring of Tyres Using Capacitance and Tuning Frequency Changes," *Smart Mater. Struct.*, 14(4), pp. 561-568.
- [12] Yilmazoglu, O., Brandt, M., Sigmund, J., Genc, E., and Hartnagel, H. L., 2001, "Integrated InAs/GaSb 3D Magnetic Field Sensors for 'the Intelligent Tire'," *Sensors and Actuators A: Physical*, 94(1-2), pp. 59-63.
- [13] Kotian, K., Headings, L. M., and Dapino, M. J., 2013, "Stress Averaging in PVDF Sensors For In-Plane Sinusoidal and Impact-Induced Stresses," *IEEE Sensors Journal*, 13(11), pp. 4444–4451.